Robotics and Autonomous Systems 62 (2014) 3–15

Contents lists available at ScienceDirect

Robotics and Autonomous Systems

journal homepage: www.elsevier.com/locate/robot

Design of a flexible tactile sensor for classification of rigid and deformable objects

Alin Drimus [a,*], Gert Kootstra [b], Arne Bilberg [a], Danica Kragic [b]

[a] Mads Clausen Institute for Product Innovation, University of Southern Denmark, 6400 Sønderborg, Denmark

[b] Centre for Autonomous Systems, School of Computer Science and Communication, Royal Institute of Technology(KTH), 100 44 Stockholm, Sweden

ARTICLE INFO

Article history:
Available online 8 August 2012

Keywords:
Tactile sensing
Piezoresistive rubber
Tactile object classification
Active perception

ABSTRACT

For both humans and robots, tactile sensing is important for interaction with the environment: it is the core sensing used for exploration and manipulation of objects. In this paper, we present a novel tactile-array sensor based on flexible piezoresistive rubber. We describe the design of the sensor and data acquisition system. We evaluate the sensitivity and robustness of the sensor, and show that it is consistent over time with little relaxation. Furthermore, the sensor has the benefit of being flexible, having a high resolution, it is easy to mount, and simple to manufacture.

We demonstrate the use of the sensor in an active object-classification system. A robotic gripper with two sensors mounted on its fingers performs a palpation procedure on a set of objects. By squeezing an object, the robot actively explores the material properties, and the system acquires tactile information corresponding to the resulting pressure. Based on a k nearest neighbor classifier and using dynamic time warping to calculate the distance between different time series, the system is able to successfully classify objects. Our sensor demonstrates similar classification performance to the Weiss Robotics tactile sensor, while having additional benefits.

1. Introduction

Research in the area of robotic grasping has gradually shifted from structured manufacturing environments toward unstructured everyday environments. Visual feedback has proven to be an important source of sensory information necessary for grasp generation and control, e.g., [1–7]. Although vision provides important information, it is not always enough or trivial to obtain. In addition, the accuracy may be limited, due to imperfect calibration and occlusions. Errors in estimation of object shape are common even for known objects and these errors may cause failures in grasping. Clearly, vision does not provide important information on object properties such as deformability or material texture.

Tactile and finger-force sensors can be used as additional sensors to improve grasping performance during grasp execution [8–10], but are still rather uncommon in practice. Mechanical compliance, for instance, is an important characteristic of an object, and it is essential in grasping fragile items. Furthermore, humans use object properties such as hardness, thermal conductivity, friction and roughness in object manipulation, which could be addressed by robotic grippers as well by using haptic feedback.

In this paper, we propose the design of a novel tactile sensor based on piezoresistive materials and conductive thread electrodes. The sensor has 8×8 taxels in an active area of 20 mm $\times$ 20 mm and is flexible being based on a piezoresistive rubber material of 0.5 mm thickness. It has high sensitivity capabilities starting from a 10 kPa pressure threshold and it provides a smooth force–resistance characteristic with little relaxation. The sensor is robust to withstand thousands of actuations without any change in its response and is moreover cheap and simple to manufacture. We demonstrate its use in a haptic-based object-classification scenario. We propose a method for classifying rigid and deformable objects using the proposed sensor. These objects cannot be discriminated based on static tactile information. We therefore apply an active exploration procedure, where a robotic gripper, equipped with the sensors, performs palpations on the objects. By squeezing the objects, the robot acquires dynamic information, which is structured through the sensory–motor coordination. This information is used to describe and classify the objects. The complete system is implemented, evaluated, and finally compared to the widely used Weiss Robotics tactile sensor [11].

This paper is organized as follows: Section 2 presents the related work regarding tactile sensors, while Section 3 describes the steps used to manufacture the proposed sensor prototype and the electronics used for data acquisition. Section 4 describes the processing of the tactile images and the data modeling needed for object classification. The experiments are presented and discussed in Section 5. The conclusions and further improvements are outlined in Section 6.

* Correspondence to: Mads Clausen Institute, University of Southern Denmark, Alsion 2, 6400 Sønderborg, Denmark. Tel.: +45 65501689.

E-mail addresses: drimus@mci.sdu.dk (A. Drimus), kootstra@kth.se (G. Kootstra), abi@mci.sdu.dk (A. Bilberg), dani@kth.se (D. Kragic).

0921-8890/$ – see front matter © 2012 Elsevier B.V. All rights reserved.
doi:10.1016/j.robot.2012.07.021

2. Related work

In this section, we first review the work on the sensor development, followed by work on tactile object classification.

In terms of tactile-array sensors for static stimuli, such as pressure, there are a range of technologies that have been used with various results [12]. There are a few technologies that can be used for manufacturing tactile-array sensors, and the most used are piezoresistive (rubbers or inks), piezocapacitive, piezoelectrical, and optical [13]. In [14], an industrial tactile-array sensor was proposed using a piezoresistive rubber. However, this sensor has a low spatial resolution and does not have any flexible capabilities. A flexible 16 × 16 sensor array with 1 mm spatial resolution was developed for minimally invasive surgery, but the sensor fails to give steady output for static stimuli, and has a high hysteresis and non-linearity [15].

A combination of static and dynamic sensors was developed in [16] to address both pressure profiles and slippage, but the design has only 4 × 7 cells, and a number of wires equal to the number of cells. Flexible sensors based on pressure conductive rubber with 3 × 16 cells were developed using a stitched electrode structure, but the construction method and the leak currents brought high variations in the measurements [17]. A flexible fingertip sensor using pressure conductive rubber was proposed in [18]. The sensor principle is based on measuring resistance of the conductive rubber from one side taking into account both small area contact resistance and the rubber resistance. The underlying layer consists of a flexible PCB, which comprises 36 pairs of gold-plated comb-shaped electrodes resulting in taxels approx. 2 mm × 2 mm.

A 32 × 32 tactile sensing array that is able to measure not only normal applied forces but also temperature has been presented in [19]. Pressure conductive rubber is employed as the tactile sensing material, and discrete temperature sensor chips are used as the temperature sensing cells. Small disks of pressure conductive rubber are bonded on predefined inter-digital copper electrode pairs which are patterned on a flexible copper–polyimide substrate, fabricated by micro-machining techniques. An approach that uses a thin film of conductive polymer instead of the conductive rubber was proposed in [20]. The material is a conductive water-based ink of a polymer that is deposited by spin-coating on a flexible plastic sheet and the electrodes were based on flex PCB or screen printing directly over the piezoresistive layer with a silver based ink.

The tactile-array sensor that we propose in this paper combines a number of benefits. The sensor, based on piezoresistive technology is flexible, which makes it easy to mount. It has furthermore high sensitivity capabilities and gives consistent measurements over time. The resolution of the sensor is high, without complex wiring. The sensor is moreover simple to produce.

Using tactile sensors for material and object recognition or classification, has become rather popular recently, as is, for instance, reflected in [21]. Different methods have been proposed to classify materials based on their texture. In [22], for instance, a learning method was proposed based on a soft anthropomorphic fingertip containing 24 randomly distributed receptors of two different kinds; strain gauges and polyvinylidene fluoride (PVDF) films. The fingertip was used to rub and push objects of different materials, like wood, paper, cork and vinyl. Based on the averages given by the strain gauges and the variance over time in the signal given by the PVDF sensors, they showed good discrimination capabilities among the considered materials.

A similar approach was employed by in [23] where the Fourier coefficients based on the dynamic measurements given by the PVDF elements and the averages from each strain gauge were used as the input for multiple classifiers. The exploration procedure involved dragging the finger across a textured surface. They showed recognition rates over 90% for eight different natural textures.

Other methods deal with object recognition and classification. In [24] the sensor presented in [22] was used and applied to a finger and the palm of a robot hand. The exploratory procedure here involved squeezing and tapping a range of seven small objects made of different materials such as cloth, paper or plastic. In their squeezing procedure, a constant pressure was applied and the average output of the strain gauges was used to classify the objects using a Kohonen self-organizing map. The method that we propose, on the other hand, uses a palpation procedure where we increase and decrease the pressure. In [25], tactile information was used to estimate whether cans and bottles are open or closed and whether they are filled. To do the classification, they designed a small number of dynamic features. In [26], multiple grasps were performed on a set of household objects in order to classify them. An unsupervised clustering method was used to learn a vocabulary from tactile observations and classification was done using a bag-of-words approach. The approach takes into consideration only tactile information at the points of contact with the considered objects. In contrast with the above method, our object classification procedure takes advantage of the complete time series, which allows more elaborate discrimination of objects.

In some studies, grasp generation is based on visual input and tactile sensing is used for closed-loop control once in contact with the object. For example, the use of tactile sensors has been proposed to maximize the contact surface for removing a book from a bookshelf [27]. The application of force, visual, and tactile feedback to open a sliding door has been proposed in [28]. Tactile information can be also used to reconstruct the shape of unknown explored objects as proposed in [29].

One of the issues often faced in household scenarios is deformable objects. Planning grasps for these types of object is not at all as well studied as rigid objects. Examples can be found in the literature, such as [30], where the deformation properties of objects are learned in order to apply suitable grasping forces for the associated objects.

Our work considers a tactile-array sensor based on piezoresistive technology. For classification, we look at the time series that the sensor provides during a full palpation procedure. Based on this dynamic information, different objects can be classified based on their tactile properties.

3. The tactile sensor

In order to construct a tactile-array sensor, we take inspiration from biology, especially in the characteristics of the human skin. Therefore, we are mainly interested in: (1) dynamic range and sensitivity, (2) size of taxels similar to the mechanoreceptor in the human hand, (3) large array size without too much wiring complexity, robustness – to withstand repeated impacts – and (4) flexibility — so that we could apply the sensor to any kind of robotic grippers very much similar to an artificial skin. Other characteristics that we are aiming for are (5) a good sensor output, (6) low complexity and simple processing circuitry, (7) ease of manufacture, and a (8) a low price. The novel tactile sensor that we propose largely achieves these goals.

3.1. Material properties

After an early investigation and testing of different technologies and methods for building tactile sensors, presented in [31], we have chosen the piezoresistive material as the most suited to build a flexible tactile-array sensor. The CSA material has shown good performance in some research works related to finger pads

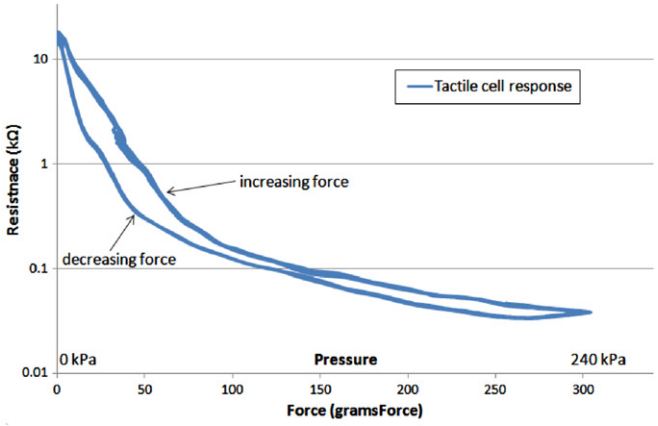

Fig. 1. Force vs. resistance characteristic for the piezoresistive material, measured over 20 trials of applying increasing and decreasing force. Note that the individual lines are hard to distinguish, because of the consistency of the sensor response.

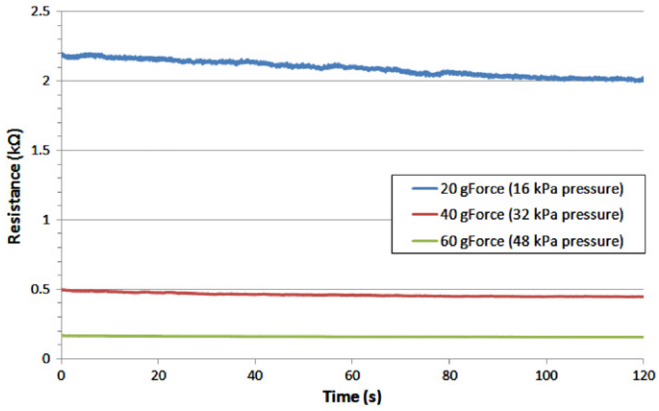

Fig. 2. Force vs. resistance characteristic for the piezoresistive material, for different static loads applied for about 2 min. Relaxation effect is more pronounced for smaller loads.

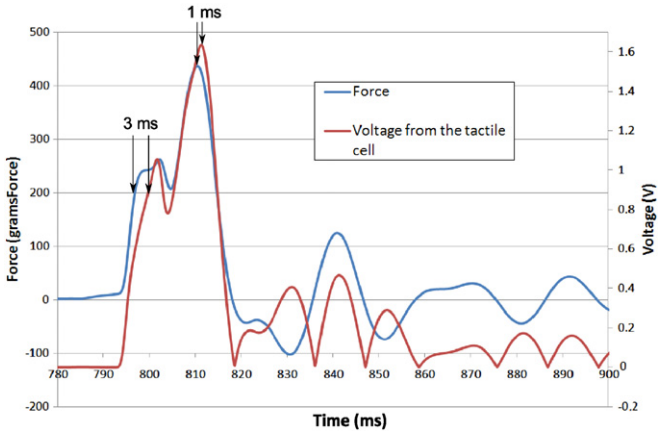

Fig. 3. Delay characteristic of the piezoresistive material when subjected to a force impulse of duration 20 ms. The rubber shows around 3 ms delay for establishing contact and 1 ms delay when releasing the contact.

for robots [15]. This pressure-sensitive conductive rubber is a material made of non-conductive elastomer, in which electric conductive particles are distributed/dispersed homogeneously. Since the electric conductive particles do not touch each other, electricity does not pass through the particles in the state when there is no external force. When external force acts, the particles come into contact with each other and more paths for a flowing current are created. According to the percolation theory [15], the distribution state of the particles, and thereby the resistance, changes as a result of producing strain in the material with external force.

The piezoresistive rubber shows an electrical resistance that ranges from about 0.5 kΩ in the compressed (on) state to several $M\Omega$ in the free (off) state. The force–resistance characteristic shows a non-linear behavior, which can be explained by the internal distribution of particles using percolation theory. Due to the elastomer nature of the base material, there is also hysteresis and creep effect. The force–resistance characteristic of the material is depicted in Fig. 1 for 20 trials. External force was applied to a test sample of the material, where the force was linearly increased up to 300 gram-force and then decreased to 0 gram-force. Taking into consideration the tip area of the actuator used to apply the force, the response for a cell ranges from approx. 10 kPa (1.5 PSI) which is the threshold sensitivity up to 250 kPa (300 PSI) being the upper limit before the saturation effect appears. Even though non-linearities and creep effects are present in the behavior of the material, we do not consider these as being a major disadvantage, as human skin also shows them [15].

There are in fact two possibilities for building electrodes around the piezoresistive material: single sided contact and double sided contact. Results presented in [31] show that a double sided electrodes method improves the sensitivity of the sensor. Therefore we have chosen to use such a structure for building the sensor. Weiss Robotics sensors are built using the single sided contact method.

Due to the relaxation effect given by the elastic properties of the piezoresistive material, the characteristic resistance is not constant over time when a force is applied to the sensor for prolonged durations of time. In order to investigate the relaxation effect of the rubber, different static loads were applied for longer periods of time (2 min), and the resistance was measured. The results for three different static loads (for 20 gram-force, 40 gram-force and 60 gram-force) are depicted in Fig. 2. The relaxation effect is more pronounced for smaller loads, as the resistance decays with approx. 10% from its initial value in the case of 20 gram-force load. The variation in the response is higher for small forces and this is because at lower strain percentage the material gets very close to the percolation threshold, therefore the rate of increase/decrease in the number of conductive chains is very high. Note that the relaxation effect is only temporary and that the sensor recovers in the order of milliseconds after the load is removed.

In order to investigate the delay response of the rubber, an impulse force pattern of 20 ms was applied normal to the surface of the taxel. Fig. 3 shows both the force applied (recorded by a load cell present in the tip of the actuator) and the voltage drop over a fixed resistor in series with the sensor (a voltage divider circuit). The delay measured reaches a maximum of 3 ms when the force is applied and goes down to 1 ms when the force is removed. It should be noted that due to mechanical inertia and the physical limitations in our actuator setup, it was impossible to generate a perfect rectangular force pattern for such short durations. A damping at changing contact conditions can be observed and this is caused by the springlike behavior of both the load cell and the sensor. These figures suggest that the material has a recovery time in the order of a few ms, which motivate an acquisition rate of hundreds of frames per second. In contrast, piezoresistive foam is expected to have a longer recovery time, due to its higher creep effect.

In terms of repeatability due to prolonged usage, the sensor exhibited no noticeable aging in the investigated experiments. Fig. 4 depicts the resistance response curves for increasing loads recorded at 11 different points in time, ranging from the first cycle of stimuli applied to the 10 000th cycle. The overlapping curves indicate that the sensor does not show significant aging due to

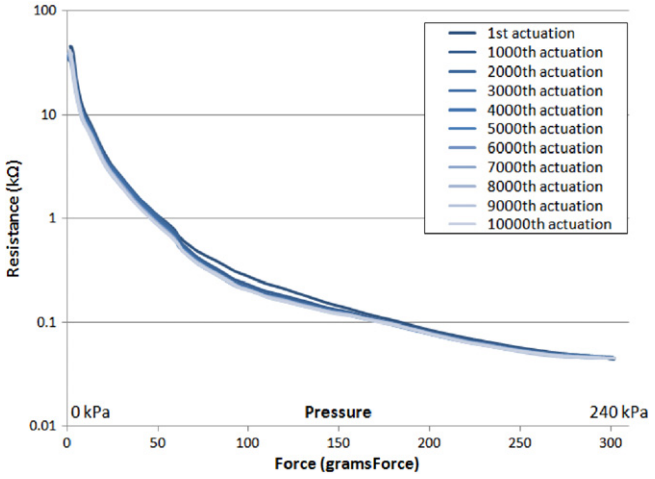

Fig. 4. Force vs. resistance characteristic after prolonged usage. Curves are plotted for increased force applied every 1000 actuations until 10 000. The response stays very consistent.

usage and that the force–resistance characteristics are consistent over time. Although not significantly, it is possible to notice that the first cycle shows the highest resistance in both low force and high force ranges, while the 10 000th cycle shows the smallest resistance. This effect may be caused by a small relaxation of the material that appears after the very first actuations are applied. Given the small variation in the characteristic and the overlapping of the curves, it is fair to assume that the response is independent of moderate usage.

Given its flexibility, cost, sensitivity, consistency, robustness, and ease of use we consider this material a very good candidate for building a tactile-array sensor.

3.2. Building the tactile sensor

One of the biggest problems when processing the information from a multi-sensor device is the wiring complexity. When a high-resolution tactile array is the aim, with n columns and m rows and considering a pair of wires for each sensing element results in $2n \cdot m$ wires, this means a complicated circuit design. Other solutions might therefore be better suited. One of them is by using electrodes arranged in rows on one side and as columns on the other side of the sensor device, as depicted in Fig. 5. In this way, by selecting only one column and one row, the information from a single element can be read. Such a readout circuit would reduce the wiring from $2nm$ to $n+m$ wires, which is a desirable improvement. This way it is possible to read a single sensor's value at a specific moment, and by iteration through all columns and rows at high speeds, all values can be read in real time.

The low complexity wiring of our sensor has the advantage that we can move the electronics away from the sensor, in contrast to, for instance, the Weiss Robotics sensor, which uses $n \cdot m + 1$ wires, forcing a design with the electronics insight the sensor. Being able to separate sensor and electronics has the advantage that the sensor stays flexible and that it can easily be replaced without having to replace the electronics, simplifying maintenance. For a different reason, the sensor used on the Barrett hand also needs to have the electronics close to the sensor, since the capacitive technology is prone to noise with long wiring.

To build a tactile-array sensor, we start with a flexible substrate made of PVC covered by an adhesive layer. On top of this substrate, we lay conductive threads spaced 2.5 mm apart in a series of eight parallel lines. On top of the threads, we add a piezoresistive rubber patch, which is 0.5 mm in thickness, and has a 20 mm × 20 mm size.

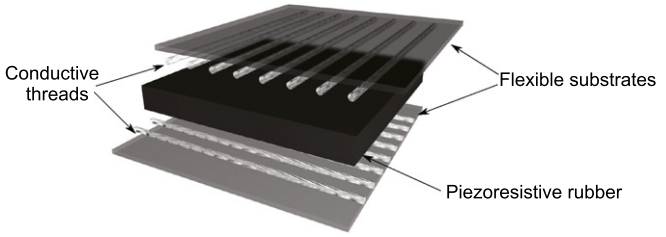

Fig. 5. Sensor structure. The piezoresistive rubber material is sandwiched between two layers with conductive threads as electrodes.

Next, a similar layer to the base layer is added on top, in such a way that the conductive threads are perpendicular to the bottom ones and face the piezoresistive material. These steps of manufacturing are illustrated in Fig. 6.

The conductive threads ensure the flexibility and maximum compliance of the whole structure. The prototype has a bend radius of 1 cm and can be mounted even on curved surfaces, given that the surface geometry can be unfolded into planar form, such as for example a cylinder. The sensor can be folded in a similar fashion as a piece of paper. Arbitrary 3D shapes cannot be covered by the sensor due to their complex geometry and to the fact that the sensor is neither stretchable nor elastic.

From our previous results [31] we have concluded that there should not be any permanent electrical contact between the electrodes and the piezoresistive rubber patch, as this reduces the sensitivity for the low-force range. This is due to the fact that the total resistance given by the sensor is composed as the sum of the contact resistance and the material resistance. When dealing with low forces, the resistance of the material will change by a small amount, while in turn, the contact resistance will account for most of the change in the output resistance. A permanent electrical contact reduces the contact resistance to a very low value, thus influencing the output sensitivity. A permanent electrical contact happens when there is a conductive gel or glue between the electrodes and the porous surface of the rubber, such that the contact resistance is significantly reduced. The conductive threads show a resistance of about 10 Ω per 10 cm, which does not affect the performance of the sensor considering the total thread length of 40 cm before the connector.

The resulting prototype is roughly 25 × 25 mm^2, 1 mm in thickness and has 64 taxels. We have manufactured larger arrays using this technique as well, but this is beyond the scope of this paper.

The robustness of our sensor is shown in Fig. 4. The lifetime of the sensor can be further increased by applying a thin and soft replaceable layer (cover) on top of the sensor. A thicker layer would reduce wear of the sensor even more, but it may affect the sensor reading by acting as a low pass filter and 'blurring' the tactile image.

A comparison of the proposed sensor with the specifications of two commercially available sensors, the Weiss Robotics DSA-9205[1] and the Barrett Hand BH8-280,[2] is made in Table 1.

3.3. Data acquisition

In this section, we describe the data acquisition process.

3.3.1. Signal conditioning

The signal conditioning for measuring the pressure applied over a tactile cell is based on the voltage divider principle. In the configuration described in Fig. 7, the sensor cell is modeling a

[1] Weiss Robotics, online manual: http://www.weiss-robotics.de/images/stories/products/dsa9205/DSA9205_08-2008_EN.pdf.

[2] Barrett Hand, online manual: http://web.barrett.com/support/BarrettHand_Documentation/BH8-280_Datasheet.pdf.

Table 1
Comparison between some commercial tactile sensors and our sensor prototype.

	Our sensor	Weiss Robotics DSA-9205	Barrett Hand BH8-280
Technology	Piezoresistive rubber	Piezoresistive foam	Capacitive
Flexibility	Flexible with 1 cm bend radius	Rigid	Rigid
Cell size	6.25 mm^2	14.44 mm^2	15 mm^2
Pressure range	10–250 kPa	250 kPa[a]	100 kPa[a]
Speed	100 fps[b]	230 fps[b]	n/a
Response delay	1–3 ms	n/a	n/a
Complexity	Low	Moderate	High

[a] Data about lower boundary is not available.
[b] Much higher frequency readout is possible with our sensor, but this would result in oversampling, since the sensor cannot respond so fast due to the creep effect of the rubber. Piezoresistive foam has a higher creep effect than rubber.

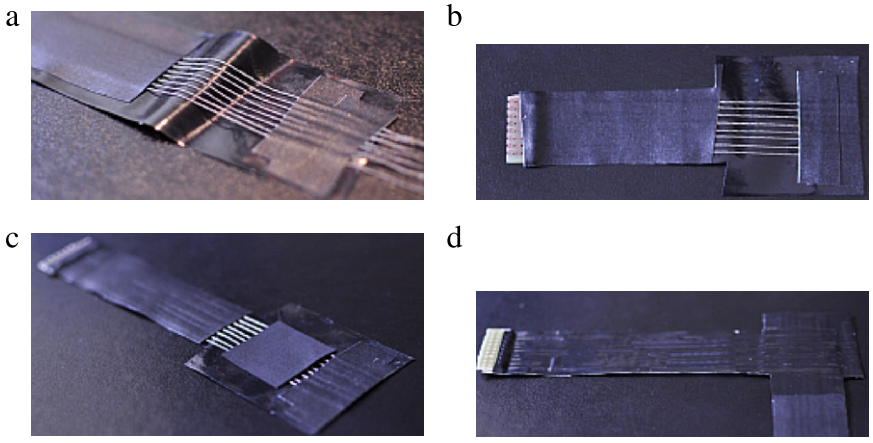

Fig. 6. Steps showing the building of the tactile sensor: (a) first layer, (b) first layer, (c) adding the piezoresistive rubber (d) the finished sensor.

variable resistor with a value of up to 50 kΩ and is connected in series with a fixed resistor — with a value typically less than 1 kΩ. The voltage is measured over this resistance as:

$$Vx = V_+ \frac{R_g}{R_{sensor} + R_g}. \quad (1)$$

Based on the above equation, a high pressure applied on the material will result in a low resistance value for the sensor, increasing the voltage drop over R_g. A low pressure applied on the material will result in a high resistance value for the sensor, therefore the voltage drop over R_g approaching 0 V.

Fig. 8 depicts the modeling of the sensor as an electrical circuit, when three columns of electrodes are placed on the bottom of the material and three rows of electrodes are placed on the top of the material. The rows feed current through the material, which is further conducted to ground over the columns. The material can be modeled as a matrix array of variable resistors, placed at each overlapping of rows and columns. The three columns are the input ports of a multiplexer, that selects only one at a time to send it further to the analog to digital conversion block. The three rows, Va, Vb and Vc are the output ports of a voltage multiplexer, that puts a V+ voltage potential at one of its outputs, according to the multiplexer control bits. If one row is addressed by the output MUX and one column is addressed by the input MUX, the voltage collected over the R_g resistance will be proportional to the resistance exhibited by the material at their overlapping.

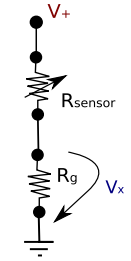

Fig. 7. Signal conditioning for measurement of one tactile cell.

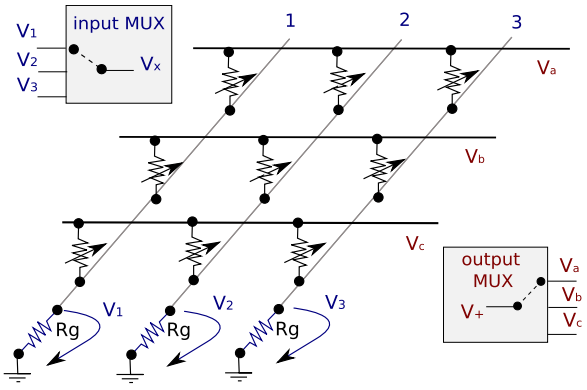

Fig. 8. Signal conditioning and voltage multiplexing for a 3 × 3 array.

3.3.2. Data acquisition

In order to achieve a high multiplexing speed and a high number of inputs we have used a dsPIC33FJ256, a 16 bit digital signal controller developed by Microchip.

Assuming an array of $n \times m$ elements arranged in n rows and m columns, the scanning procedure works as follows: for each row_i from $(row_1, \ldots, row_n)$ we apply a voltage over the row_i ($V_{applied}$) and all the others are kept to ground (0 V). We use n Digital Output ports $(O_1, \ldots, O_n)$ to control which row will be enabled and which not, by setting $O_i = 1$ and all others $O_1, \ldots, O_{i-1}, O_{i+1}, \ldots, O_n = 0$. Setting all other rows to 0 will have the benefit of avoiding phantom effects. The phantom effect usually consists in seeing a high value for a point when three adjacent neighbors have high val-

1. Rubber ball
2. Balsam bottle
3. Rubber duck
4. Empty bottle
5. Full bottle
6. Bad orange
7. Fresh orange
8. Joggling ball
9. Tape
10. Wood block

Fig. 9. Objects used in the experimental evaluation.

ues. At this point, we use m analog input ports ($I_1, \ldots, I_m$) corresponding to the m columns, $col_1, \ldots, col_m$. We start by converting the voltage on I_1 by ADC, followed by the conversion of the I_2 and so forth, until we reach I_m. After this point we have obtained m values, $V_{i1}, V_{i2}, \ldots, V_{im}$ that represent the voltage differences between row_i and all m columns. Doing so will result in a matrix of $n \times m$ voltage readings. Each such matrix represents a frame or a *tactile image*.

The implemented data-acquisition module scans tactile arrays of up to 512 cells, providing 100 fps, with eight bit data for each taxel. In our case, the module was used to scan the 64 taxels of the sensor and provide a tactile image every 10 ms.

4. Object classification

To illustrate the use of our sensor, we apply it to an object classification task. The goal of the application is for a robot to classify ten rigid and deformable objects that are shown in Fig. 9 based on tactile information. In order to do so, the robot actively explores the objects using a palpation procedure by squeezing the objects. By doing so, the tactile sensors are stimulated, which results in a sequence of measurements. This sequence is then used to recognize which object is palpated. Note that this is only possible through active perception, since a static reading of tactile information is not sufficient to classify the object under inspection. It is necessary to look at the dynamic sensory patterns resulting from the motor action.

4.1. Palpation procedure

During the experiments, the objects were manually placed in between the gripper jaws. The palpation procedure started by closing the gripper's fingers until contact was established. This was then followed by a squeeze procedure, in five small steps, each step squeezing the object 1 mm. Squeezing stiffer objects requires the use of more force, which translates to the increase of the current used by the gripper to perform the action. If the object cannot be further squeezed due to its stiffness, then the gripper will use its maximum rated force to squeeze it and this will be propagated onto the sensor, which will react accordingly, giving maximum output. After these squeeze steps, five de-squeeze steps of 1 mm each were executed, and then the gripper released the object. The force applied by the gripper at its jaws is dependent on the material properties of the grasped object. The whole palpation procedure lasted about 6–7 s, depending on the object's size.

4.2. Hardware setup

The hardware setup consisted of a Schunk PowerCube Robotic Arm with a 1-DOF Schunk PG70 parallel gripper as the end effector (see Fig. 12). The parallel jaws were equipped with our tactile sensors, and then further connected to the data-acquisition circuitry as described in the previous section. The data-acquisition modules stream the data over USB to a host computer that records the tactile data and controls the execution of the grasp procedure.

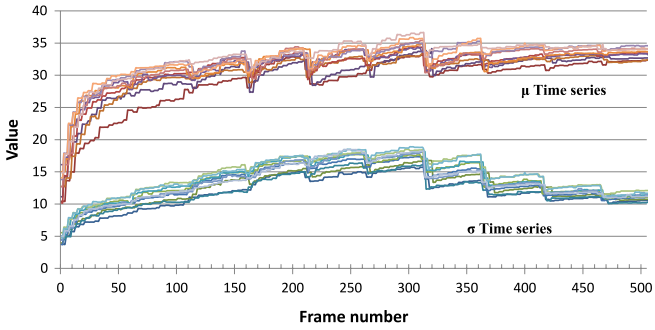

Fig. 10. Different series for μ (red) and σ (blue) describing the palpation procedures of the *Full bottle* object. The graphs show that the different time series are consistent despite squeezing the object at different positions. (For interpretation of the references to colour in this figure legend, the reader is referred to the web version of this article.)

4.3. Data modeling

The start of a palpation procedure (time $t = 0$) is considered when both gripper jaws are in contact with the object, which is given when the tactile-sensor data is above a specified threshold. The procedure ends at time $t = N$, where N represents the number of frames (tactile images) recorded from the tactile sensors. In our case the data-acquisition system provides a tactile image each 10 ms. Examples of such tactile images are illustrated in Fig. 11 for a few grasped objects, being sampled every 1 s from a palpation procedure. Because the execution time varies slightly for each experiment, the number of tactile images in each sequence varies between 500 and 520. A tactile image is an array of $M = 64$ values (8×8), $v_1, v_2, \ldots, v_M$, each representing an eight bit value that encodes the pressure applied over the taxel. Considering around 500 frames for each sensor during an exploration procedure, we obtain a high-dimensional description of each palpation procedure. In order to reduce the dimensionality, we extract just the first two moments of each tactile image as two independent features. The first feature corresponds to the average of an image, given by:

$$\mu = \frac{1}{M} \sum_{i=1}^{M} v_i, \tag{2}$$

and the second feature corresponds to the standard deviation of the pixels in an image, given by:

$$\sigma = \sqrt{\frac{1}{M} \sum_{i=1}^{M} (v_i - \mu)^2}. \tag{3}$$

The average of the tactile image gives a good estimate of the overall pressure applied to the contact area, which increases with the number of contact taxels and with the pressure over each taxel. The standard deviation is a rough estimate of the number of contact pixels, describing a wider or narrower contact area. These two features reduce the dimensionality of the data to N values for each feature. An observation Z is therefore represented as:

$$Z_\mu = \{\mu_1, \mu_2, \ldots, \mu_N\} \tag{4}$$

$$Z_\sigma = \{\sigma_1, \sigma_2, \ldots, \sigma_N\}. \tag{5}$$

In Fig. 10, different time series depicting the μ and σ sequences for the *Full bottle* object are represented.

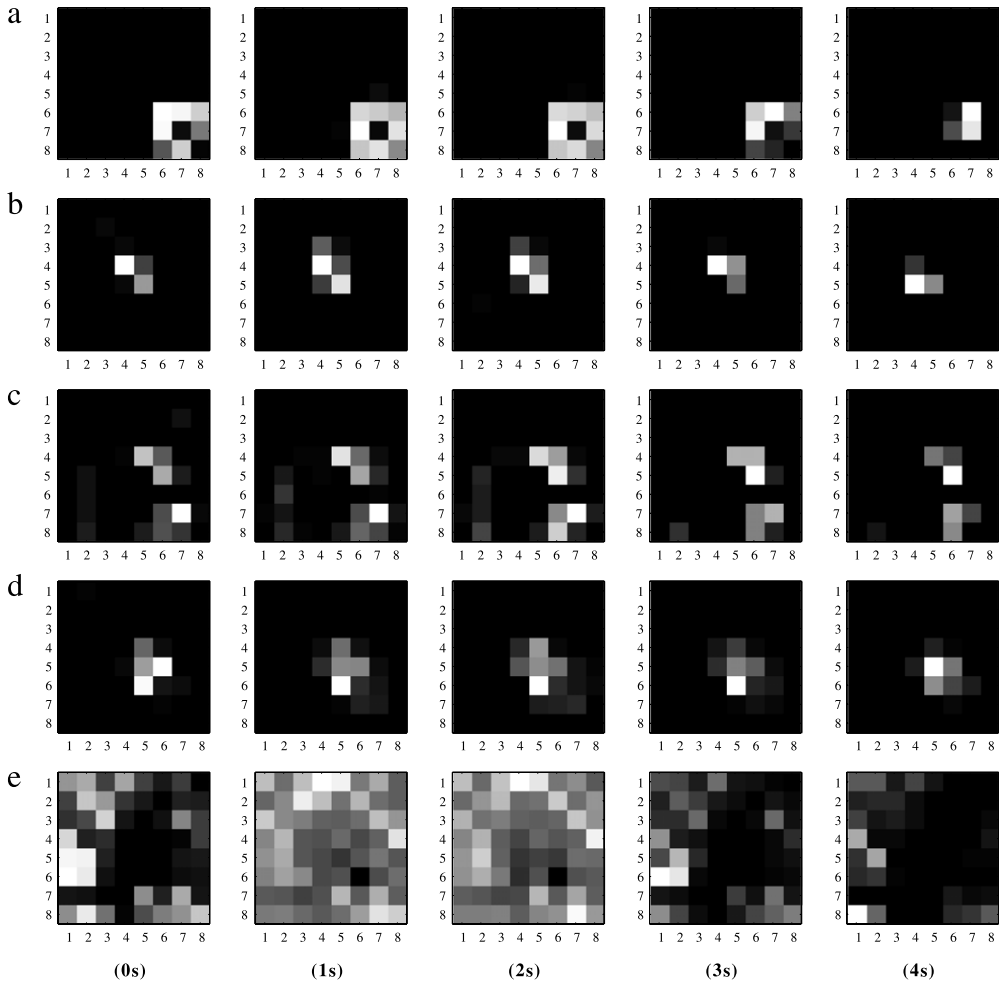

Fig. 11. Example tactile images for a few grasped objects, sampled every 1 s during the palpation procedure: (a) *Rubber ball*, (b) *Duck*, (c) *Bad orange*, (d) *Fresh orange* and (e) *Tape*.

4.4. Classification and distance metric

We use a k nearest neighbors (kNN) classification method to classify the time series resulting from the palpation procedure. A number of training examples are stored for each object. A new observation is compared to the training data. Based on a distance metric, the k nearest neighbors are found, and the new observation is assigned the label that is most frequent in this set.

In order to calculate the distance between the time series, we use the Dynamic Time Warping algorithm [32], which is widely used in different areas for measuring the similarity between time series by minimizing the effects of distortion and shifts in time or speed. This is important in our case, since we are dealing with real-world perception and action, which both are noisy. The sequences are "warped" non-linearly in time to determine a measure of their similarity independent of certain non-linear variations in the time dimension. It allows an elastic transformation and can be used to detect similarity between signals with different phases. Given two time series, $X = \{x_1, x_2, \ldots, x_N\}$ and $Y = \{y_1, y_2, \ldots, y_M\}$, the DTW algorithm returns the distance, $d = \mathrm{DTW}(X, Y)$, between the two time series, where $d \in \mathbb{R}$, $d > 0$ and with d being closer to 0 for more similar time series and larger otherwise.

One palpation procedure results in an observation, z, which consists of μ and σ time series for both fingertip sensors:

$$z = \{Z_{\mu,l}, Z_{\mu,r}, Z_{\sigma,l}, Z_{\sigma,r}\} \tag{6}$$

where $Z_{\mu,l}, Z_{\mu,r}, Z_{\sigma,l}, Z_{\sigma,r} \in [0, 255]^N$ represent the time series of features computed for the images of the left, l, and right, r, sensor.

In the experiments, we consider different classification methods, based on different distance metrics. The simplest distance metric is based only on the first moment of the sensor on one of the fingertips, e.g., $Z_{\mu,l}$, to measure the distance between z_1 and z_2:

$$d_{l,1}(z_1, z_2) = \mathrm{DTW}\left(Z^1_{\mu,l}, Z^2_{\mu,l}\right) \cdot w_{\mu,l} \tag{7}$$

where $w_{\mu,l}$ is used for normalization, so that DTW distance is scaled between 0 and 1.

An improved metric is given by also taking into consideration the second feature:

$$d_{l,2}(z_1, z_2) = \mathrm{DTW}\left(Z^1_{\mu,l}, Z^2_{\mu,l}\right) \cdot w_{\mu,l} + \mathrm{DTW}\left(Z^1_{\sigma,l}, Z^2_{\sigma,l}\right) \cdot w_{\sigma,l} \tag{8}$$

where, $w_{\mu,l}$ and $w_{\sigma,l}$ normalize the values of the respective DTW distances, so that both features get equal importance in the combined distance measure.

The same two distance metrics can be written for the right sensor as well, resulting in $d_{r,1}(z_1, z_2)$ and $d_{r,2}(z_1, z_2)$.

When considering both sensors, the distance metric can be calculated using only the first feature of both sensors:

$$d_{lr,1}(z_1, z_2) = d_{l,1}(z_1, z_2) + d_{r,1}(z_1, z_2), \tag{9}$$

or by taking into consideration both features:

$$d_{lr,2}(z_1, z_2) = d_{l,1}(z_1, z_2) + d_{r,1}(z_1, z_2) + d_{l,2}(z_1, z_2) + d_{r,2}(z_1, z_2). \tag{10}$$

The different distance metrics are used for our classification algorithm, using the k nearest neighbor classifier.

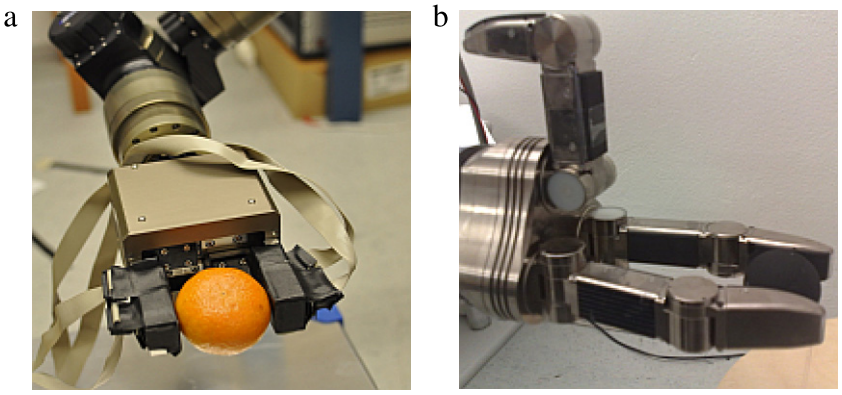

Fig. 12. Experimental setup (a) using the Schunk Parallel Gripper with our sensor, (b) using the Schunk Dexterous Hand with Weiss sensors.

5. Experimental evaluation

5.1. Experiment 1: Object classification

For testing our sensor, we have recorded tactile data for 10 various household objects, rigid and deformable, some of them being similar in shape and size to the others (see Fig. 9). The set of objects consisted of a rubber ball, a balsam bottle, a rubber duck, an empty 0.5 l plastic bottle, a full 0.5 l plastic bottle, a bad orange, a fresh orange, a juggling ball, a tape roll and a small block of wood. The tape roll and the block of wood are rigid objects, while the others were more or less deformable. Each palpation procedure was repeated around 10 times for each object, and the grasping was executed each time with the object slightly moved or rotated in the gripper jaws, to ensure some variability in the data set. We thus obtained a data set, $\mathcal{D}$, of $|\mathcal{D}| = 97$ labels for 10 objects. The classification algorithm was based on three kNN classifiers, with $k = \{1, 3, 5\}$. As explained in Section 4.4, we apply different distance metrics to take into account the tactile readings from the left sensor, from the right sensor, and from both sensors. Moreover, the first moment, or the first two moments are used in the distance calculation.

In order to quantify the classification performance, we use a 10-fold cross validation, where we split $\mathcal{D}$ into 10 disjoint subsets, $\mathcal{D}_i$, each having approximately the same number of examples per object, in order to ensure equal training for each label. Each subset is used as a test set, $\mathcal{D}_{\text{test}} = \mathcal{D}_i$ where all the other nine subsets are used as training data, $\mathcal{D}_{\text{train}} = \mathcal{D} - \mathcal{D}_{\text{test}}$. The recognition rate of each subset $\mathcal{D}_i$ is given by the number of correctly classified labels divided by the total number of tests. We thus obtain 10 recognition rates, one for each fold, $\{r_1, r_2, \ldots, r_{10}\}$, which we use to calculate the mean and 95% confidence intervals for the recognition results.

5.2. Classification results

The recognition rates for using one feature (the first moment) for classification are shown in Table 4. It can be seen that the recognition rates differ depending on which sensor is used. This is mostly based on the fact that the sensors were placed on the gripper jaws in a non-perfect alignment and because of small differences between the sensors which are due to the manual manufacturing of the sensors. Using both sensors instead of only one improves the performance significantly. This shows that the two sensors complement each other and make the system more robust. There are no significant differences in recognition performance when a larger k is used in the kNN classifier. This means that we can reduce the computational complexity of the classifier by only considering the first-nearest neighbor without the loss of performance.

Table 4 also shows the results when two features (first and second moment) are used for classification. Compared to using only one feature, the recognition rates are higher. This and the fact that the difference in performance between the two sensors disappeared shows that the addition of the second feature improves the robustness of the system. Again, no significant differences can be seen for the different values of k in the classifier.

Table 2 shows the resulting confusion matrices for 1-NN classification based on left, right and both sensors, using one feature, and Table 3 shows the same using two features. The numbers on the axes correspond to the object numbers given in Fig. 9. The vertical axis shows the truth and the classification made by the system is given on the horizontal axis. In general, it can be observed from the clear diagonal that the classification performs nicely. However, some objects are sometimes wrongly classified, generally for objects that have similar material properties. The tape (9) and wood block (10), two hard and solid objects, for instance, are sometimes mixed up. Other understandable examples are the balsam bottle (2), which is classified as either an empty bottle (4) or a bad orange (6), and a mix-up between the bad orange (6) and the juggling ball (8), which both are objects that are more plastic than elastic, meaning they do not go back to their initial shape that easy.

An interesting comparison is between the bad orange (6) and the fresh orange (7). It can be appreciated from the tactile image examples in Fig. 11 that the fresh orange does not become soft as easily and its stiffness determines a more concentrated contact area as well as peak pressure compared to a bad orange. However, bad oranges and fresh oranges are also sometimes hard to distinguish using this method because unless the bad oranges are strongly damaged, they still have a minor elastic behavior and vice-versa, the fresh oranges have a plastic behavior after a few palpation procedures.

5.3. Comparison with the Weiss Robotics sensor

We compare our sensor with the Weiss Robotics tactile sensor [11,14], since this is a widely used sensor for tactile feedback. We therefore investigate if we can obtain similar results using our sensor. The Weiss Robotics tactile sensors are mounted on the Schunk Dexterous Hand SDH and they consist of 13 rows $\times$ 6 columns of taxels, in about 24 mm $\times$ 51 mm area (see Fig. 12). The area occupied by this sensor is almost double compared to the sensor that we propose, therefore a different resolution is achieved. Increasing the geometrical resolution of our sensor would mean the addition of detail data for the extra cells. Such details could be used for improvement of recognition if the objects were small enough to actually benefit from a more precise contact shape. Given the fact that the objects are rather big with respective to

Table 2
Confusion matrix for 1-NN classification for the proposed sensors: using one feature. The vertical axis represents the truth and the horizontal represents the output of the classification. The labels correspond to the test objects.

Left sensor

obj	1	2	3	4	5	6	7	8	9	10
1	**100**	0	0	0	0	0	0	0	0	0
2	0	**83.3**	0	0	0	16.7	0	0	0	0
3	0	0	**58.3**	8.3	0	0	33.3	0	0	0
4	0	0	0	**100**	0	0	0	0	0	0
5	0	0	0	0	**100**	0	0	0	0	0
6	0	0	0	0	0	**76.9**	0	23.1	0	0
7	0	0	9.1	0	0	9.1	**72.7**	9.1	0	0
8	0	0	0	0	0	37.5	0	**62.5**	0	0
9	0	0	0	0	0	0	0	0	**62.5**	37.5
10	0	0	0	0	0	0	0	0	37.5	**62.5**

Right sensor

obj	1	2	3	4	5	6	7	8	9	10
1	**90.9**	0	9.1	0	0	0	0	0	0	0
2	0	**50**	0	33.3	0	16.7	0	0	0	0
3	0	8.3	**66.7**	0	16.7	0	8.3	0	0	0
4	0	10	0	**90**	0	0	0	0	0	0
5	0	0	0	0	**100**	0	0	0	0	0
6	0	0	0	0	0	**84.6**	0	15.4	0	0
7	0	0	0	0	0	0	**100**	0	0	0
8	0	0	0	0	0	12.5	0	**87.5**	0	0
9	0	0	0	0	0	0	0	0	**87.5**	12.5
10	0	0	0	0	0	0	0	0	12.5	**87.5**

Both sensors

obj	1	2	3	4	5	6	7	8	9	10
1	**100**	0	0	0	0	0	0	0	0	0
2	0	**83.3**	0	0	0	16.7	0	0	0	0
3	0	0	**83.3**	0	0	0	16.7	0	0	0
4	0	10	0	**90**	0	0	0	0	0	0
5	0	0	0	0	**100**	0	0	0	0	0
6	0	0	0	0	0	**84.6**	0	15.4	0	0
7	0	0	9.1	0	0	0	**90.9**	0	0	0
8	0	0	0	0	0	0	0	**100**	0	0
9	0	0	0	0	0	0	0	0	**100**	0
10	0	0	0	0	0	0	0	0	12.5	**87.5**

Table 3
Confusion matrix for 1-NN classification for the proposed sensors: using two features. The vertical axis represents the truth and the horizontal represents the output of the classification. The labels correspond to the test objects.

Left sensor

obj	1	2	3	4	5	6	7	8	9	10
1	**100**	0	0	0	0	0	0	0	0	0
2	0	**66.7**	0	0	0	33.3	0	0	0	0
3	0	0	**91.7**	0	0	0	8.3	0	0	0
4	0	0	0	**100**	0	0	0	0	0	0
5	0	0	0	0	**100**	0	0	0	0	0
6	0	0	0	0	0	**92.3**	0	7.7	0	0
7	0	0	9.1	0	0	0	**81.8**	9.1	0	0
8	0	0	0	0	0	12.5	0	**87.5**	0	0
9	0	0	0	0	0	0	0	0	**62.5**	37.5
10	0	0	0	0	0	0	0	0	12.5	**87.5**

Right sensor

obj	1	2	3	4	5	6	7	8	9	10
1	**81.8**	0	18.2	0	0	0	0	0	0	0
2	0	**66.7**	0	16.7	0	16.7	0	0	0	0
3	8.33	0	**91.7**	0	0	0	0	0	0	0
4	0	10	0	**90**	0	0	0	0	0	0
5	0	0	0	0	**100**	0	0	0	0	0
6	0	0	0	0	0	**76.9**	7.7	15.4	0	0
7	0	0	0	0	0	9.1	**90.9**	0	0	0
8	0	0	0	0	0	12.5	0	**87.5**	0	0
9	0	0	0	0	0	0	0	0	**100**	0
10	0	0	0	0	0	0	0	0	12.5	**87.5**

Both sensors

obj	1	2	3	4	5	6	7	8	9	10
1	**100**	0	0	0	0	0	0	0	0	0
2	0	**83.3**	0	0	0	16.7	0	0	0	0
3	0	0	**91.7**	0	0	0	8.3	0	0	0
4	0	20	0	**80**	0	0	0	0	0	0
5	0	0	0	0	**100**	0	0	0	0	0
6	0	0	0	0	0	**92.3**	0	7.7	0	0
7	0	0	0	0	0	18.2	**81.8**	0	0	0
8	0	0	0	0	0	25	0	**75**	0	0
9	0	0	0	0	0	0	0	0	**100**	0
10	0	0	0	0	0	0	0	0	12.5	**87.5**

the size of one cell and because of the dimensionality reduction, this resolution difference would not influence the comparison in classification results between the two sensors. However, other applications could benefit from more detailed data regarding contact shapes.

We tested the Weiss sensor using the same experimental setup. Again we test the recognition performance on the 10 objects, each object with 10 observations. After processing the recorded tactile data according to the same algorithms as described for our sensor, we obtained a similar data set of time series of features.

The results shown in Table 5 suggest that our sensor performs similarly to the Weiss sensor. Using our classification procedure it is also possible to discriminate with high recognition rates between the chosen objects using the Weiss sensor. Looking at the differences between left and right sensors, the experiments show that the Weiss sensors are also prone to manufacturing and placement differences. This is caused by the sensitivity of the specific sensor used, which was rather low, caused probably by manufacturing or wear and tear of the sensor during its use with the robotic hand.

Table 4
Classification results using the proposed sensor for one and two features. The averages and 95 % confidence intervals are obtained using 10-fold cross-validation.

*k*NN	Left sensor (%)	Right sensor (%)	Both sensors (%)
Using one feature			
1NN	78.14 ± 4.55	86.00 ± 6.90	91.57 ± 3.89
3NN	76.14 ± 6.86	86.00 ± 6.32	88.00 ± 4.64
5NN	70.71 ± 5.40	84.00 ± 6.90	84.00 ± 6.32
Using two features			
1NN	88.57 ± 5.18	88.00 ± 6.07	92.00 ± 4.64
3NN	87.00 ± 6.23	85.00 ± 6.93	90.00 ± 5.54
5NN	78.14 ± 7.69	85.00 ± 6.93	91.00 ± 5.15

Table 5
Classification results using Weiss Robotics sensors, for one and two features using 10-fold cross-validation, 95 % confidence interval.

*k*NN	Left sensor (%)	Right sensor (%)	Both sensors (%)
Using one feature			
1NN	87.00 ± 6.23	75.00 ± 6.35	91.00 ± 6.47
3NN	85.00 ± 6.35	69.00 ± 3.34	88.00 ± 8.22
5NN	81.00 ± 7.04	67.00 ± 4.84	84.00 ± 7.94
Using two features			
1NN	93.00 ± 4.84	74.00 ± 7.44	92.00 ± 4.64
3NN	88.00 ± 7.23	72.00 ± 7.74	85.00 ± 7.96
5NN	84.00 ± 6.32	69.00 ± 5.15	84.00 ± 7.44

Table 6
Comparison between our proposed sensors (output combined from left and right fingers) and Weiss Robotics sensors.

*k*NN	Our sensor (%)	Weiss Robotics (%)	Difference (%)
Using one feature			
1NN	91.57 ± 3.89	91.00 ± 6.47	0.57
3NN	88.00 ± 4.64	88.00 ± 8.22	0.00
5NN	84.00 ± 6.32	84.00 ± 7.94	0.00
Using two features			
1NN	92.00 ± 4.64	92.00 ± 4.64	0.00
3NN	90.00 ± 5.54	85.00 ± 7.96	6.00
5NN	91.00 ± 5.15	84.00 ± 7.44	7.00

For convenience of comparison, the classification results using our sensor and the Weiss sensor are given in Table 6. The table shows that our sensor performs similarly well, if not slightly better, compared to the Weiss sensor.

The confusion matrices shown in Tables 7 and 8 show that the recognition results are in general good, pointed out by the clear diagonal. However, surprisingly, rigid and soft objects were sometimes mixed up, such as the wood block (10) and the balsam bottle (2), the tape (9) and the rubber ball (1), and the balsam bottle (2) and the wood block (10).

The sensitivity of the Weiss sensors is the limiting factor because it delays the start of the palpation procedure to the point where the object is already deformed, whereas our sensor is more sensitive and can therefore acquire more information from the object palpation.

Even though we achieve similar recognition rates using our sensor, we have obtained rather different results in the confusion matrix, where we could see that deformable objects such as good oranges, bad oranges and juggling balls were confused more often amongst each other, whereas rigid objects, like the tape and the wood block, were only confused with other rigid objects. This difference in behavior is based on the higher sensitivity of our sensor.

The mistakes made by this method while using our sensor are more sensible and desired. It shows that differences in the time series between objects with similar material properties are small, whereas differences between objects with different properties are larger. To improve the performance, we will have to add additional features that highlight the more subtle differences among objects.

5.4. Experiment 2: Classification of fruits and vegetables

The aim of this experiment is to demonstrate the ability of our sensitive sensor to recognize deformable objects (fruits and vegetables) with a high degree of confidence based on the haptic feedback from the 8 × 8 sensors during the palpation procedure. Seven different fruits and vegetables with very similar material properties were used in this experiment. Fig. 13 shows the experimental setup.

In this experiment, the palpation takes 8 s and consists of squeezing the object for 4 s and de-squeezing the objects for the other 4, closing and opening the gripper in a continuous movement at 1 mm/s. The data-acquisition system provides a tactile image each 20 ms, thus in total about 400 frames. For each object, 10 palpations were done, resulting in 70 trials in total. Fig. 14 shows different time series depicting the μ and σ sequences for the kiwi fruit.

The recognition rates for using one feature, the first moment, and both features, first and second moments, are shown in Table 9. Despite the fact that the objects have very similar material properties, the recognition rates are high, especially when both features are used. Table 10 gives the confusion matrices (the vertical axis represents the truth and the horizontal represents the output of the classification). The clear diagonal for both one and two features confirms the successful recognition. The classification based on only one feature shows some mistakes, noticeably the grape that was sometimes mistaken for a mushroom and the lime

Table 7
Confusion matrix for 1-NN classification for the Weiss Robotics sensors: using one feature. The vertical axis represents the truth and the horizontal represents the output of the classification. The labels correspond to the test objects.

Left sensor

obj	1	2	3	4	5	6	7	8	9	10
1	**90**	0	0	0	0	0	10	0	0	0
2	0	**80**	0	0	0	0	0	0	0	20
3	0	0	**100**	0	0	0	0	0	0	0
4	0	0	0	**90**	10	0	0	0	0	0
5	0	10	0	0	**80**	0	0	0	0	10
6	0	0	0	0	0	**100**	0	0	0	0
7	8.3	0	0	0	8.3	16.7	**66.7**	0	0	0
8	0	0	0	0	0	0	0	**100**	0	0
9	0	0	0	0	0	0	0	0	**100**	0
10	0	22.2	0	0	11.1	0	0	0	0	**66.7**

Right sensor

obj	1	2	3	4	5	6	7	8	9	10
1	**70**	0	20	0	0	0	0	0	10	0
2	0	10	0	**50**	0	0	0	0	0	40
3	0	0	**90**	0	0	10	0	0	0	0
4	0	0	0	**100**	0	0	0	0	0	0
5	0	0	0	10	**60**	0	0	10	10	10
6	0	0	20	0	0	**80**	0	0	0	0
7	8.3	0	8.3	0	0	0	**83.3**	0	0	0
8	0	0	0	0	0	0	0	**100**	0	0
9	11.1	0	0	0	22.2	0	0	0	**66.7**	0
10	0	22.2	0	0	0	0	0	0	0	**77.8**

Both sensors

obj	1	2	3	4	5	6	7	8	9	10
1	**90**	0	10	0	0	0	0	0	0	0
2	0	**80**	0	0	0	0	0	0	0	20
3	0	0	**100**	0	0	0	0	0	0	0
4	0	0	0	**90**	10	0	0	0	0	0
5	0	0	0	10	**90**	0	0	0	0	0
6	0	0	0	0	0	**100**	0	0	0	0
7	0	0	0	0	8.3	8.3	**83.3**	0	0	0
8	0	0	0	0	0	0	0	**100**	0	0
9	11.1	0	0	0	0	0	0	0	**88.9**	0
10	0	11.1	0	0	0	0	0	0	0	**88.9**

Table 8
Confusion matrix for 1-NN classification for the Weiss Robotics sensors: using two features. The vertical axis represents the truth and the horizontal represents the output of the classification. The labels correspond to the test objects.

Left sensor

obj	1	2	3	4	5	6	7	8	9	10
1	**90**	0	0	0	0	0	10	0	0	0
2	0	**80**	0	0	0	0	0	0	0	20
3	0	0	**100**	0	0	0	0	0	0	0
4	0	0	0	**90**	10	0	0	0	0	0
5	0	0	0	0	**100**	0	0	0	0	0
6	0	0	0	0	0	**100**	0	0	0	0
7	0	0	8.33	0	0	0	**83.3**	8.3	0	0
8	0	0	0	0	0	0	0	**100**	0	0
9	0	0	0	0	0	0	0	0	**100**	0
10	0	11.1	0	0	0	0	0	0	0	**88.9**

Right sensor

obj	1	2	3	4	5	6	7	8	9	10
1	**80**	0	10	0	0	0	0	0	10	0
2	0	10	0	**50**	0	0	0	0	0	40
3	0	0	**90**	0	0	10	0	0	0	0
4	0	0	0	**100**	0	0	0	0	0	0
5	10	0	10	10	**60**	0	0	0	10	0
6	0	0	10	0	0	**90**	0	0	0	0
7	8.3	0	0	0	0	8.3	**66.7**	8.3	8.3	0
8	0	0	0	0	0	0	0	**100**	0	0
9	22.2	0	0	0	11.1	0	11.1	0	**55.6**	0
10	0	22.2	0	0	0	0	0	0	0	**77.8**

Both sensors

obj	1	2	3	4	5	6	7	8	9	10
1	**100**	0	0	0	0	0	0	0	0	0
2	0	**80**	0	0	0	0	0	0	0	20
3	0	0	**100**	0	0	0	0	0	0	0
4	0	0	0	**100**	0	0	0	0	0	0
5	0	0	0	10	**90**	0	0	0	0	0
6	0	0	0	0	0	**100**	0	0	0	0
7	8.3	0	0	0	0	0	**83.3**	8.3	0	0
8	0	0	0	0	0	0	0	**100**	0	0
9	11.1	0	11.1	0	0	0	0	0	**77.8**	0
10	0	11.1	0	0	0	0	0	0	0	**88.9**

Table 9
Classification results for one and two features using 10-fold cross-validation, 95 % confidence interval, for the tested objects: grape, kiwi, lime, mushroom, orange, plum and tomato.

*k*NN	One feature (%)	Two features (%)
1NN	74.29 ± 6.63	92.86 ± 5.94
3NN	68.57 ± 6.63	88.57 ± 6.63
5NN	61.43 ± 10.51	84.29 ± 4.77

that was sometimes classified as an orange. However, with the addition of the second feature, only a few mix-ups took place.

6. Conclusions and discussion

We presented a novel tactile-array sensor, described the design and the sensor properties, and applied the sensor to two classification tasks based on the tactile feedback during a palpation procedure. We showed that the sensor is sensitive, is consistent over time, shows little relaxation, and is robust to a large number of force applications. The sensor furthermore has the advantageous properties of being flexible, having a high resolution, being easy to mount, and being simple to produce.

Table 10
Confusion matrix for 1NN classification for the test objects using data from both sensors combined. The vertical axis represents the truth and the horizontal represents the output of the classification. The labels correspond to the test objects: (1) *Grape*, (2) *Kiwi*, (3) *Lime*, (4) *Mushroom*, (5) *Orange*, (6) *Plum* and (7) *Tomato*.

One feature

obj	1	2	3	4	5	6	7
1	20	0	20	**40**	0	0	20
2	0	**90**	0	0	0	0	10
3	0	0	**70**	0	30	0	0
4	10	0	0	**90**	0	0	0
5	0	0	0	0	**80**	0	20
6	0	0	10	0	0	**90**	0
7	10	0	0	0	20	0	**70**

Two features

obj	1	2	3	4	5	6	7
1	**80**	0	0	20	0	0	0
2	0	**100**	0	0	0	0	0
3	0	0	**100**	0	0	0	0
4	10	0	0	**90**	0	0	0
5	0	0	0	0	**90**	0	10
6	10	0	0	0	0	**90**	0
7	0	0	0	10	0	0	**90**

To demonstrate the use of the proposed sensor, we applied it in an active object-classification method. In the application, two sensors are mounted on both fingers of a robotic gripper. In order to classify an object, the robot performs a palpation procedure, that is, it squeezes and de-squeezes the object. By actively exploring the object in this way, the system acquires a sequence of tactile measurements for both fingers. Each measurement consists of the first and second moments of the 8×8 tactile image. We applied a k nearest neighbor classification method using dynamic time warping to measure the distance between two time series. An advantage of this procedure is that the robot acquires knowledge about the objects from its own experience, through its own sensory–motor system, making prior calibration unnecessary.

This object-classification method was tested in two experiments. In the first experiment, the system needed to classify ten different household objects, while in the second experiment seven different fruits and vegetables were used. Both experiments reveal that the classification performance improves when the sensors on both fingers and both features are used. In the first experiment, we compare our sensor to the Weiss Robotics tactile sensor. We demonstrated that our sensor performs equally well while having some additional benefits, which will be discussed below. Interestingly, we observed that the classification using the Weiss sensor sometimes mixed up objects with different material properties, while the errors made using our sensor are more sensible, mixing up objects with similar material properties. In the second experiment, the robot needed to classify different objects with similar material properties, in order to demonstrate the sensitivity of our sensor. The results show that the system performs very well.

We are satisfied that our sensor shows similar performance to the Weiss Robotics sensor, which is widely used. In addition, our

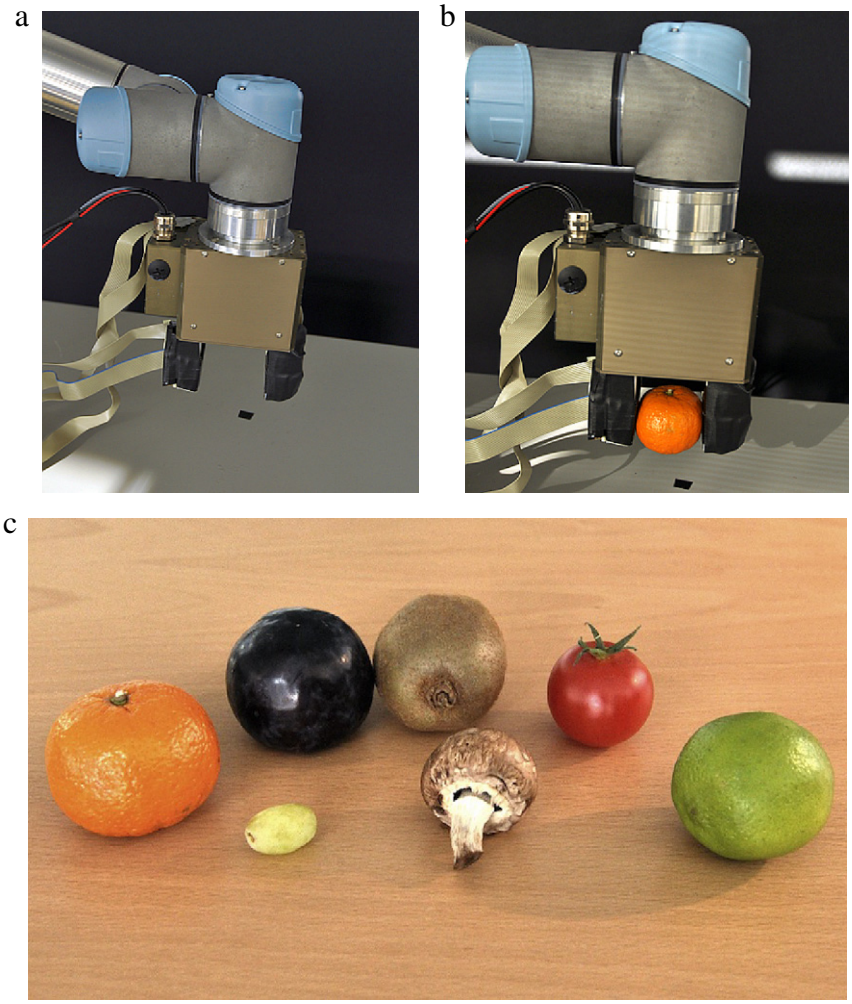

Fig. 13. Experimental setup. (a) Sensors mounted on the Schunk Parallel Gripper, (b) gripper performing the palpation of an orange and (c) the objects considered for palpation.

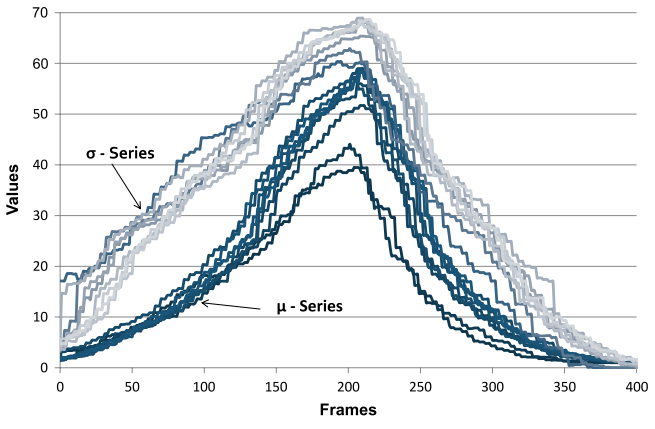

Fig. 14. Different series for μ (dark blue) and σ (light blue) describing the palpation procedures of the kiwi fruit. The graphs show that the different time series are consistent despite squeezing the object at different positions. (For interpretation of the references to colour in this figure legend, the reader is referred to the web version of this article.)

sensor has a number of benefits. It is flexible and thin, and therefore can be mounted on any kind of robotic grippers or fingers. The output shows a good response for pressure ranges above 10 kPa. It is robust to withstand thousands of actuations without any change in its response and has an increased spatial resolution. Being cheap and simple to manufacture makes it easy and inexpensive to replace after it gets damaged. We are confident that our sensor can be successfully used in other robotic applications such as grasping unknown objects and determining physical characteristics of these objects, such as stiffness and texture.

The mistakes that the classification method makes using our sensor, are sensible. Objects with similar material properties are sometimes mixed up. This means that the distance measures using our sensor make sense. Furthermore, we believe that we can take even more advantage of the high sensitivity of our sensor for the classification tasks by using higher-level features that emphasize the more subtle differences in the tactile-array readings in addition to the first two moments that we used in this paper.

The sensor described has a bandwidth of 100 Hz per taxel, which is sufficient for applications that deal with force control and, as we have shown in this paper, provides enough information about the material properties of objects. While valuable slip information could be extracted from the 100–400 Hz range in the frequency domain, sensors based on piezoresistive technologies are not the best candidates. Other approaches propose simplified methods (piezoelectric-based vibration sensors have been successfully used due to their high bandwidth and increased sensitivity for very small variations in the forces applied). Such sensors could be used to analyze texture information, slip phenomena or dynamic conditions of contact [15].

In order to improve classification performance, vision can be used as complementary to tactile sensing. The tactile sensors can

sense material properties, such as elasticity, which cannot be observed visually. Vision, on the other hand provides important information on the visual appearance and shape, and can be used to sense from a distance. Combining both modalities will improve classification performance. The benefit of combining visual and tactile information has been show, for instance, in [33].

Acknowledgments

This work is supported by the Danish Handyman Project, by the EU through the EMICAB (IST-FP7-IP-270182) and eSMCs (IST-FP7-IP-270212) projects and Swedish Foundation for Strategic Research.

References

[1] A. Saxena, J. Driemeyer, A.Y. Ng, Robotic grasping of novel objects using vision, International Journal of Robotics Research 27 (2) (2008) 157–173.
[2] R. Detry, E. Baseski, M. Popovic, Y. Touati, N. Krueger, O. Kroemer, J. Peters, J. Piater, Learning continuous grasp affordances by sensorimotor exploration, in: O. Sigaud, J. Peters (Eds.), From Motor Learning To Interaction Learning in Robots, Springer-Verlag, Berlin, Germany, 2010, pp. 451–465.
[3] K. Huebner, K. Welke, M. Przybylski, N. Vahrenkamp, T. Asfour, D. Kragic, R. Dillmann, Grasping known objects with humanoid robots: A box-based approach, in: Proceedings of the 14th International Conference on Advanced Robotics, Munich, Germany, 2009.
[4] B. Rasolzadeh, M. Bjorkman, K. Huebner, D. Kragic, An active vision system for detecting, fixating and manipulating objects in real world, International Journal of Robotics Research 29 (2–3) (2010) 133–154.
[5] M. Popovic, D. Kraft, L. Bodenhagen, E. Baseski, N. Pugeault, D. Kragic, T. Asfour, N. Kruger, A strategy for grasping unknown objects based on co-planarity and colour information, Robotics and Autonomous Systems 58 (5) (2010) 551–565.
[6] J. Bohg, D. Kragic, Learning grasping points with shape context, Robotics and Autonomous Systems 59 (4) (2010) 362–377.
[7] M. Popović, G. Kootstra, J.A. Jørgensen, D. Kragic, N. Krüger, Grasping unknown objects using an early cognitive vision system for general scene understanding, in: Proceedings of the IEEE/RSJ International Conference on Intelligent Robots and Systems (IROS), 2011, pp. 987–994.
[8] M. Shimojo, T. Araki, A. Ming, M. Ishikawa, A high-speed mesh of tactile sensors fitting arbitrary surfaces, IEEE Sensors Journal 10 (4) (2010) 822–830.
[9] M. Higashimori, M. Kaneko, A. Namiki, M. Ishikawa, Design of the 100 g capturing robot based on dynamic preshaping, International Journal of Robotics Research 24 (9) (2005) 743–753.
[10] Y. Bekiroglu, D. Kragic, V. Kyrki, Learning grasp stability based on tactile data and HMMs, in: Proceedings of the 19th IEEE International Symposium in Robot and Human Interactive Communication, Viareggio, 2010, pp. 132–137.
[11] Weiss robotics tactile sensor. [Online] http://www.weiss-robotics.de/en.html.
[12] M. Lee, H. Nicholls, Tactile sensing for mechatronics — a state of the art survey, Mechatronics 9 (1999) 1–32.
[13] M. Cutkosky, R. Howe, W. Provancher, Force and tactile sensors, in: Handbook of Robotics, Springer, 2008, pp. 455–476.
[14] K. Weiss, H. Wörn, The working principle of resistive tactile sensor cells, in: Mechatronics and Automation, 2005 IEEE International Conference, Vol. 1, 2005, pp. 471–476.
[15] P. Goethals, Tactile feedback for robot assisted minimally invasive surgery: an overview, Tech. Rep., K.U. Leuven, July 2008.
[16] D. Göger, N. Gorges, H. Woern, Tactile sensing for an anthropomorphic robotic hand: Hardware and signal processing, in: Proceedings of the IEEE International Conference on Robotics and Automation, Kobe, 2009, pp. 895–901.
[17] M. Shimojo, A. Namiki, M. Ishikawa, R. Makino, K. Mabuchi, A tactile sensor sheet using pressure conductive rubber with electrical-wires stitched method, IEEE Sensors Journal 4 (5) (2004) 589–596.
[18] Y.-F. Zhang, Y.-W. Liu, M.-H. Jin, H. Liu, Design of a finger-tip flexible tactile sensor for an anthropomorphic robot hand, in: H. Liu, H. Ding, Z. Xiong, X. Zhu (Eds.), Intelligent Robotics and Applications, in: Lecture Notes in Computer Science, vol. 6424, Springer, Berlin, Heidelberg, 2010, pp. 762–773.
[19] Y.-J. Yang, M.-Y. Cheng, S.-C. Shih, X.-H. Huang, C.-M. Tsao, F.-Y. Chang, K.-C. Fan, A 32 × 32 temperature and tactile sensing array using pi-copper films, The International Journal of Advanced Manufacturing Technology 46 (2010) 945–956.
[20] J. Castellanos-Ramos, R. Navas-González, H. Macicior, T. Sikora, E. Ochoteco, F. Vidal-Verdú, Tactile sensors based on conductive polymers, Microsystem Technologies 16 (2010) 765–776.
[21] R. Dahiya, G. Metta, G. Cannata, M. Valle, Guest editorial special issue on robotic sense of touch, IEEE Transactions on Robotics 27 (3) (2011) 385–388.
[22] K. Hosoda, Y. Tada, M. Asada, Anthropomorphic robotic soft fingertip with randomly distributed receptors, Robotics and Autonomous Systems 54 (2) (2006) 104–109.
[23] N. Jamali, C. Sammut, Majority voting: material classification by tactile sensing using surface texture, IEEE Transactions on Robotics 27 (3) (2011) 508–521.
[24] S. Takamuku, G. Gomez, K. Hosoda, R. Pfeifer, Haptic discrimination of material properties by a robotic hand, in: IEEE 6th International Conference on Development and Learning ICDL, 2007, pp. 1–6.
[25] S. Chitta, M. Piccoli, J. Sturm, Tactile object class and internal state recognition for mobile manipulation, in: Proceedings of the IEEE International Conference on Robotics and Automation, Anchorage, AK, 2010, pp. 2342–2348.
[26] A. Schneider, J. Sturm, C. Stachniss, M. Reisert, H. Burkhardt, W. Burgard, Object identification with tactile sensors using bag-of-features, in: Proceedings of the IEEE/RSJ International Conference on Intelligent Robots and Systems, St. Louis, MO, 2009, pp. 243–248.
[27] A. Morales, M. Prats, P. Sanz, A.P. Pobil, An experiment in the use of manipulation primitives and tactile perception for reactive grasping, in: Science and Systems, Workshop on Robot Manipulation: Sensing and Adapting to the Real World, Atlanta, USA, 2007.
[28] M. Prats, P. Sanz, A. del Pobil, Vision-tactile-force integration and robot physical interaction, in: IEEE International Conference on Robotics and Automation, Kobe, Japan, 2009, pp. 3975–3980.
[29] A. Bierbaum, M. Rambow, T. Asfour, R. Dillmann, A potential field approach to dexterous tactile exploration, in: Proceedings of the IEEE/RAS International Conference on Humanoid Robots (Humanoids), Daejeon, 2008, pp. 360–366.
[30] A.M. Howard, G.A. Bekey, Intelligent learning for deformable object manipulation, Autonomous Robots 9 (1) (2000) 51–58.
[31] A. Drimus, N. Marian, A. Bilberg, Tactile sensing for object identification, in: Proceedings of the International Workshop on Research and Education in Mechatronics, Glasgow, UK, 2009.
[32] H. Sakoe, S. Chiba, Dynamic programming algorithm optimization for spoken word recognition, IEEE Transactions on Acoustics, Speech and Signal Processing 26 (1) (1978) 43–49.
[33] Y. Bekiroglu, R. Detry, D. Kragic, Learning tactile characterizations of object- and pose-specific grasps, in: IEEE/RSJ International Conference on Intelligent Robots and Systems, 2011. http://dx.doi.org/10.1109/IROS.2011.6094878.

Alin Drimus is a PhD student in Robotics at the Mads Clausen Institute at the University of Southern Denmark. In 2008 he obtained an MSc degree in Electronics and Information Technology from the Technical University of Cluj-Napoca, Romania. The MSc project was developed at the University of Nice, Sophia Antipolis, France in the field of ubiquitous computing. His research is in the area of biologically inspired tactile sensors and tactile data processing and interpretation.

Gert Kootstra is a post-doctoral researcher at the Center for Autonomous Systems at the Royal Institute of Technology (KTH) in Stockholm. His current research interests are in perception for robotic grasping and manipulation. He received his PhD in Artificial Intelligence from the University of Groningen, the Netherlands in 2009 on the topic of visual attention and active vision. From 2002 to 2005, he was a junior lecturer in Robotics and Autonomous Systems at the Artificial Intelligence Institute at the University of Groningen.

Arne Bilberg is an associate Professor and Head of the Mechatronics group at the Mads Clausen Institute in Sønderborg, a part of the University of Southern Denmark. He received an MSc in Mechanical Engineering, from the Technical University of Denmark. In 1989 he obtained a PhD degree in Computer Integrated Manufacturing. From 1990 to 1991 he was visiting Professor at the State University of New York, USA and from 1995 appointed associate Professor at the Institute of Process and Production Engineering, Technical University of Denmark. From 1998 he was employed as a Technology Architect with the company Linak A/S, where he worked on implementing new actuator technologies. He was appointed associate Professor at University of Southern Denmark in 2004. His research is in the area of mechatronics, product innovation and manufacturing.

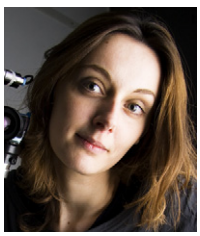

Danica Kragic is a Professor at the School of Computer Science and Communication at KTH in Stockholm. She received an MSc in Mechanical Engineering from the Technical University of Rijeka, Croatia in 1995 and a PhD in Computer Science from KTH in 2001. Danica received the 2007 IEEE Robotics and Automation Society Early Academic Career Award. She is chairing the IEEE RAS Technical Committee on Computer and Robot Vision and since 2009 has served as an IEEE RAS AdCom member. Her research is in the area of computer vision, object grasping and manipulation and human–robot interaction.